# Deformation and Breakup of Micro- and Nanoparticle Stabilized Droplets in Microfluidic Extensional Flows

Molly K. Mulligan and Jonathan P. Rothstein*

Department of Mechanical and Industrial Engineering, University of Massachusetts, 160 Governors Drive, Amherst, Massachusetts 01003, United States

ABSTRACT: Using a microfluidic flow-focusing device, mono-disperse water droplets in oil were generated and their interface populated by either 1 μm or 500 nm amine modified silica particles suspended in the water phase. The deformation and breakup of these Pickering droplets were studied in both pure extensional flow and combined extensional and shear flow at various capillary numbers using a microfluidic hyperbolic contraction. The shear resulted from droplet confinement and increased with droplet size and position along the hyperbolic contraction. Droplet deformation was found to increase with increasing confinement and capillary number. At low confinements and low capillary numbers, the droplet deformation followed the predictions of theory. For fully confined droplets, where the interface was populated by 1 μm silica particles, the droplet deformation increased precipitously and two tails were observed to form at the rear of the droplet. These tails were similar to those seen for surfactant covered droplets. At a critical capillary number, daughter droplets were observed to stream from these tails. Due to the elasticity of the particle-laden interface, these drops did not return to a spherical shape, but were observed to buckle. Although increases in droplet deformation were observed, no tail streaming occurred for the 500 nm silica particle covered droplets over the range of capillary numbers studied.
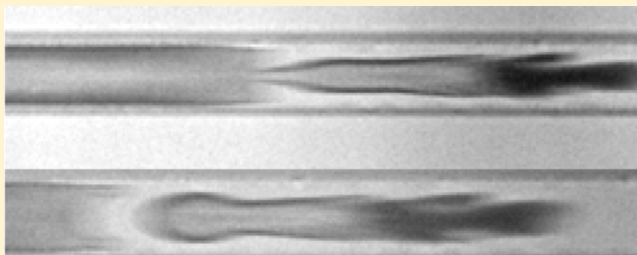
INTRODUCTION

Emulsions are common in our everyday lives and can be found in food, personal care products, and pharmaceuticals and can be used as microreactors.[1] Emulsion droplets are readily deformable under flow because the liquid—liquid interface is mobile unlike solid particles.[2,3] Also, unlike solid particles, emulsion droplets can coalesce. For that reason, the droplets within emulsions are commonly stabilized against coalescence with the addition of surfactants or solid particles.[4] Solid particles, unlike surfactants, do not assemble into aggregates in the bulk, but they can assemble at the liquid—liquid interface where, due to their size, they are held more strongly than surfactants.[4] Particle stabilized emulsions, commonly called Pickering emulsions, have attracted a great deal of attention for their potential use in creating new materials, medications where they can act as agents to deliver drugs, and cosmetics.[5,6] The understanding of emulsion droplet deformation under flow has been of interest since Taylor's seminal experiments on droplet deformation.[7] A number of studies investigated droplet deformation and breakup in both shear and extensional flows using shear rheometers, four roll mills, and microfluidic devices.[8,9] In many of these experiments, the role of confinement on the deformation of a single droplet was investigated as a first approximation of the flow environment that a droplet would experience in a concentrated emulsion.[9,10] In this work, we will utilize a microfluidic hyperbolic contraction that can impose a nearly uniaxial extensional flow over a wide range of extension rates and degrees of droplet confinement.

Although many of these studies have investigated the deformation and breakup of droplets stabilized by surfactants, the study of the deformation of the droplets of Pickering emulsions under flow has not yet been performed. Understanding the dynamics of particle laden droplet deformation and breakup is important to a large number of industries and commercial applications as mentioned above. Rheology of bulk Pickering emulsions has shown that particle stabilized emulsions are shear-thinning[11] and that oil—oil droplets stabilized by particles are prevented from coalescing under shear. However, at a high enough particle concentration, threads covered in particles begin to form.[12]

Pickering[13] demonstrated how solid particles stabilize emulsions by residing at the interface of an oil droplet in a continuous water phase. A particle's ability to stabilize an emulsion depends on the particles' wettabilty, shape, concentration, and interparticle interactions. For spherical particles, the energy needed to remove a particle from the interface between the two liquid phases is

$$E = \pi r_p^2 \sigma (1 \pm \cos \theta)^2 \tag{1}$$

where r_p is the radius of the particle. In eq 1, the positive sign corresponds to the removal of the particle into the continuous phase and the minus is for the removal of the particle into the

dispersed phase.[14] It is interesting to note that particle stabilization was exploited by the food industry, even before the dynamics of particle stabilization were well understood, by using ice crystals in ice cream and fat particles in whipping cream.[4] A variety of different materials can be used to make particles for emulsion stabilization including fumed silica, latex, polystyrene, calcite, and cadmium—selenium nanoparticles.[5,15−18] In addition, bioparticles such as ferritin, which is a spherical protein, have been shown to be quite effective at stabilizing these emulsions.[19]

Recently, a method was developed to measure the adsorption energy of self-assembled nanoparticles at the oil—water interface by monitoring the interfacial tension of the system during particle self-assembly.[20] It was also found that the binding energy of these systems could be tuned with the addition of salt and/or choice of solvent.[20] In some instances, salt can also be used to control the aggregation of colloidal particles on planar interfaces by screening surface charges of the particles and the interface.[17] The self-assembly of colloidal particles at the interface between two immiscible fluids is driven by the reduction of interfacial energy between the two phases.[4,21,22] Recently, however, several groups have reported not observing a reduction in the interfacial tension when particles are present on the interface between the two phases,[15] so this seems to be an open question in the literature.

Many emulsions are prepared using high-speed mixing and agitation, which produces a polydisperse emulsion. As an example, Wang et al.[5] created Pickering-type emulsions by shaking an oil—water mixture and stabilizing the droplets against coalescence with calcite particles. More recently, microfluidic droplet creation methods have been developed to create monodisperse emulsions.[23−27] In the experiments described here, a microfluidic flow focusing device of the design presented by Mulligan and Rothstein[9] will be used to generate monodisperse droplets for a series of Pickering emulsion studies.

Once the droplets have been created, it takes a finite amount of time for the interface to become fully populated with particles. This time scale is governed by the diffusion of particles through a fluid as they are subjected to Brownian motion. The diffusion coefficient for a spherical particle, $D_{diffusion}$, is

$$D_{diffusion} = \frac{k_B T}{6\pi\eta_c r_p} \tag{2}$$

where k_B is the Boltzmann constant, T is the temperature, and η_c is the viscosity of the fluid in which the particles are suspended.[28] From this a conservative estimate of the time for the particles to diffuse to the interface can be approximated by

$$t \approx \frac{x^2}{D_{diffusion}} \tag{3}$$

where x is the distance the particle must diffuse to the surface. In our system, this time scale is several seconds.

In the case where the liquid—liquid interface becomes saturated with particles, the interface can become solid because the particles become jammed and immobile. Emulsion droplets with solid elastic shells are called colloidosomes, and they have been utilized in a wide variety of encapsulation applications.[29,30] Colloidosomes are formed by emulsifying a suspension of two immiscible fluids along with colloidal particles. Once the droplet interface is completely covered, the resulting elastic shell has a well-defined permeability and easily measured mechanical properties.[29] Dinsmore et al.[29] showed that the material properties can be tuned by varying the size and/or type of particle used. Sander et al.[30] showed that microfluidic devices could be used to create monodisperse colloidosomes with a wide variety of surface properties which can be tuned by the choice of functionalized nanoparticles populating the surface of the colloidosomes.

Droplet formation, as well as droplet deformation and breakup, is governed by the interplay between the viscous and interfacial forces between the continuous and dispersed phase fluids. This interplay is characterized by the capillary number

$$Ca = \frac{U\eta_c}{\sigma_{12}} = \frac{\dot{\varepsilon}R\eta_c}{\sigma_{12}} \tag{4}$$

where U is the velocity, R is the maximum radius of the drops that do not break, η_c is the viscosity of the continuous phase, $\dot{\varepsilon}$ is the extension rate, and σ_{12} is the interfacial tension between the dispersed and continuous phases. Droplet deformation is defined as

$$D = \frac{a - b}{a + b} \tag{5}$$

where a is the semimajor axis of an ellipse and b is the semiminor axis of the ellipse. If a critical capillary number is reached, the droplet will break up. The critical capillary number for droplet breakup under shear and extensional flows was well characterized by Bentley and Leal,[31] who noted that the critical capillary number for droplet breakup is a function of the type of flow, shear, or extension used to deform the droplets and also the viscosity ratio, $\lambda = \eta_d/\eta_c$, where η_d is the viscosity of the dispersed phase. In extensional flows, the critical capillary number for droplet breakup is smaller than that for shear flow.[31] The deformation of clean droplets as well as droplets with surfactants have been well studied under various flow conditions, including irrotational flows,[31] shear flows,[7,32] extensional flows,[31] and combined shear and extensional flows.[8,9]

As seen in the report by Mulligan and Rothstein,[9] microfluidics lends itself well to the study of individual droplet deformation and breakup. Microfluidic devices can be designed to make monodisperse, bidisperse, and even polydisperse emulsions using a variety of droplet formation techniques.[26] These droplets can then be subjected to a variety of flow types downstream of droplet formation. The deformation and breakup of individual Pickering emulsion droplets in extensional flows has never before been studied. In this work, microfluidic techniques were used to look at individual particle coated droplet deformation under extensional and then mixed extensional and shear flows utilizing a hyperbolic contraction.

■ EXPERIMENTAL SECTION

The experimental flow cell is shown in Figure 1a. In these microfluidic devices, a steady stream of monodisperse droplets is created using flow focusing techniques. Droplets are created upstream of a hyperbolic contraction where droplet deformation is measured as a function of extension rate and confinement. Particles which were suspended in the dispersed aqueous phase were given sufficient time to populate the interface of the droplets. Devices were fabricated using standard soft lithography techniques[33,34] and the process described in detail in our previous work.[9]

Flow of the continuous and dispersed phases was driven by two stepper-motor actuated microsyringe pumps (New Era Pump System, NE-500 OEM) using a 1 mL plastic syringe (BD, plastic Leur-Lok Tip) for the dispersed phased and a 10 mL plastic syringe (BD, plastic Leur-Lok Tip) for the continuous phase. All experiments were carried out on
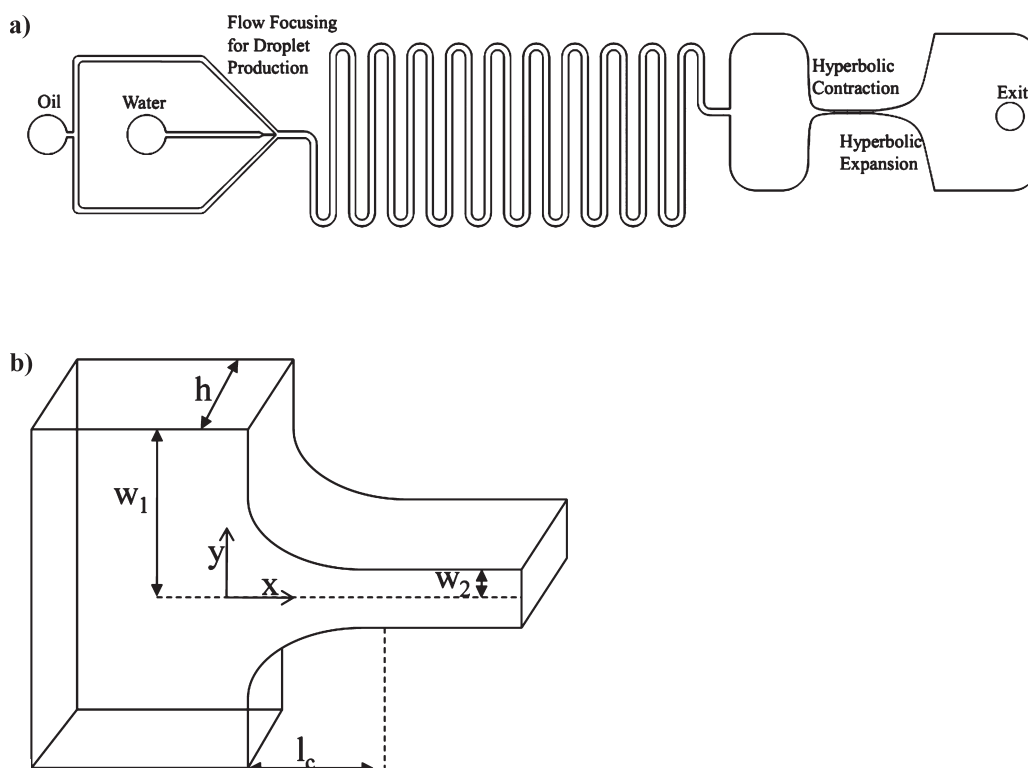
a)

b)

Figure 1. Schematic diagram of the microfluidic flow cell used in this work. (a) The entire flow cell can be seen, including the flow focusing device, the numerous turns used to give the particles time to populate the droplet interface, and the hyperbolic contraction. (b) Close up of the hyperbolic contraction used to create a uniform uniaxial extensional flow along the center line of the channel with all of the relevant dimensions labeled.

an inverted microscope (Nikon TE2000-U), and video data was recorded using a high-speed video camera (Vision Research, Phantom 4.6). The continuous phase fluid for all experiments was Miglyol 840 (Miglyol 840, Sasol) which has a viscosity of η_c = 10 mPa·s. The dispersed phase consisted of either a 3.4% suspension of 1 μm diameter amine modified silica microspheres (Polysciences, Inc.) or a 3.0% suspension of 500 nm diameter amine modified silica microspheres (Polysciences, Inc.). The viscosity ratio, $\lambda = \eta_d/\eta_c$, was fixed at λ = 0.1. The interfacial tension between Miglyol oil 840 and the 3.4% suspension of 1 μm particles was measured to be 7.1 mN/m and for the 3.0% suspension of 500 nm particles it was 15.3 mN/m. All interfacial tension measurements were made using a pendent drop experiment (Dataphysics, OCA 20, San Jose, CA).

A hyperbolic contraction was chosen to study droplet deformation under extensional flow and to investigate the role of confinement on droplet deformation because it can be used to achieve a nearly constant extensional flow along the centerline of the contraction.[35] Extensive details of the hyperbolic contraction geometry can be found in previous work.[9,36] The hyperbolic contraction is shown schematically in Figure 1b with all of the relevant dimensions labeled. After reaching its minimum width, the contraction is extended for an additional distance at a separation of $2w_2$, where w_2 is the final downstream half-width of the contraction, so that the effect of confinement on droplet deformation can be observed, where confinement is defined as

$$C = \frac{r_d}{w_2} \tag{6}$$

where r_d is the radius of the droplet. Shown in Table 1 are the relevant dimensions of the two flow cells used. The contraction is then re-expanded through a hyperbolic expansion designed to result in a compression rate 10 times smaller than that of the contraction.

Table 1. Dimensions for Each of the Flow Cells Used in the Experiments

	w_1 (μm)	w_2 (μm)	l_c (μm)	extension (μm)	c_1 (mm^2)
FC1	3000	50	1000	1500	0.025
FC2	6000	75	1500	2000	0.056

The extension rate in the channel is calculated from the volumetric flow rate, input into the computer controlled syringe pumps, and geometric parameters

$$\dot{\varepsilon} = \frac{\partial u}{\partial x} = \frac{Q}{c_1 h} \tag{7}$$

where Q is the volumetric flow rate, h is the height of the channel, and the design parameter $c_1 = (1/2)w_2 l_c$ is related to w_2 and l_c the length of the contraction.

In our microfluidic device, a range of extension rates between 90 s$^{-1} < \dot{\varepsilon} <$ 2300 s^{-1} were accessible. Additionally, the total Hencky strain imposed on the fluid can be determined from $\varepsilon = \ln(w_1/w_2)$ which for our geometry is equal to ε_{FC1} = 4.1 and ε_{FC2} = 4.4. The extension rate calculated from eq 7 was used to recalculate an extensional capillary number from eq 6.

■ RESULTS AND DISCUSSION

The deformation of Pickering emulsion droplets with 1 μm diameter particles populating the oil—water interface is shown in Figure 2 as a function of capillary number for a broad range of droplet confinements. Scanning electron microscopy images of the particles were taken to verify that the particles were discrete particles and not chains of particles, which would affect the
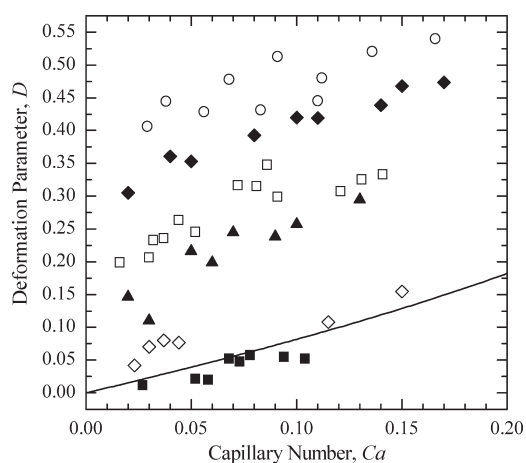
Figure 2. Deformation parameter as a function of the extensional capillary number at various confinements for 1 μm amine modified silica particle coated droplets in oil. Data includes confinements of $C = 0.6$ (■), $C = 0.9$ (◇), $C = 1.1$ (▲), $C = 1.2$ (□), $C = 1.4$ (◆), and $C = 1.6$ (○). The line is a prediction of droplet deformation when droplets are not confined.

packing dynamics of the particles as well as the elasticity and rigidity of the particle shell formed on the droplets. Each point in Figure 2 is averaged over multiple drops with the same confinement and capillary number. All droplets are measured at the end of the hyperbolic channel just after it passes into the straight channel. For unconfined clean water droplets, in a continuous oil phase, with a viscosity ratio of $\lambda = 0.1$, the critical capillary number for droplet breakup is predicted to be $Ca_{cr} = 0.19$.[31] Mulligan and Rothstein[9] recently showed that confinement and the resulting shear from the walls of the hyperbolic contraction can significantly increase the deformation of water and surfactant covered droplets at the same capillary number. Similar results are observed here for the particle covered droplets. In Figure 2, the droplet deformation increases monotonically for any given confinement from left to right between capillary numbers of $0.02 \leq Ca \leq 0.18$. For the moderately confined case of $C = 0.6$, the line for the droplet deformation as a function of capillary number lies close to the line of droplet deformation without confinement predicted by the Maffetone and Minale model,[37] while the case of $C = 0.9$ shows a modest increase over the Maffetone and Minale model. These trends were also observed for unconfined water and surfactant droplets.[9] Surfactant coated droplets were seen to deviate from the predictions of the Maffetone and Minale model at a confinement of $C = 0.8$ due to the droplets transitioning from the predicted ellipsoidal deformation to bulletlike shapes and eventually to tail streaming.[9] Tail streaming will be discussed in more detail later in this paper. The Maffetone and Minale model was used to predict droplet deformation in the absence of confinement for homogeneous uniaxial extensional flow. The model assumes the droplets remain ellipsoidal and do not break up; therefore, it is only truly valid at moderate to low capillary numbers. A detailed discussion of the Maffetone and Minale model and how it relates to droplet deformation can be found in refs 9 and 37. For fully confined droplets, $C \geq 1$, the droplet deformation is found to deviate quickly from the predictions of the Maffetone and Minale model. Droplet deformation increases monotonically with capillary number even in the presence of confinement; however, as droplet confinement increases, larger droplet deformations are seen

for a given capillary number. These trends are similar to those noted for water and surfactant droplet deformation within a hyperbolic contraction, although for surfactant covered droplets deviation from the Maffetone and Minale model is observed even for confinements of $C < 1.0$.[9]

Droplet deformation was seen to increase with increasing confinement beyond $C > 0.6$ for all capillary numbers tested. For droplets which are fully confined, $C \geq 1$, the initial droplet radius is larger than the final half-width, w_2, of the downstream contraction and the droplets are too large to fit through the contraction without deforming. Therefore, even in the absence of flow, these droplets would be deformed solely due to confinement. As observed by Mulligan and Rothstein,[9] all data was found to lie above the predicted droplet deformation at zero capillary number due to confinement effects alone. However, it is important to note that the observed droplet deformation is not solely due to the presence of the contraction walls, nor is it a superposition of the steric deformation and the deformation due to a purely extensional flow as predicted by the Maffetone and Minale model and observed for unconfined droplets. The droplet deformation is due to a complex interplay between the extensional and shear flow in the hyperbolic contraction, and we will see that, for the fully confined case, the result is a shape transition in the particle laden droplets. Shape transitions were also observed for surfactant coated droplets deformed by extensional flows and mixed extensional and shear flow conditions within a hyperbolic contraction.[9]

Particle image velocimetry measurements have shown that, for the hyperbolic contraction, the velocity profile is relatively flat across the channel. As a result, across roughly the inner 80% of the channel width, the velocity is nearly constant and can be approximated as plug flow. However, the presence of shear near the walls can play an important role in droplet deformation especially for fully confined or the nearly fully confined droplets.[9,35] The shear rate is at a maximum near the walls and vanishes at the centerline of the contraction. At the narrowest points in the contraction, the shear rate can be twice as much as the extension rate; however, shear rate decreases significantly at wider points of the contraction. The significance of shear increases as droplet confinement increases due to the proximity of the droplet edge to the walls of the contraction.

Shown in Figure 3 are a series of images of a partially confined droplet, $C = 0.9$, and two fully confined droplets, $C = 1.1$ and $C = 1.3$, traveling through the hyperbolic contraction at various capillary numbers. For the partially confined droplet (Figure 3a–e), a gradual shape transition from an ellipsoidal shape to a flat trailing droplet edge, bulletlike shape is observed as the capillary number increases from $0.06 \leq Ca \leq 0.2$. For the fully confined droplet, over the same range of capillary numbers, the shape transition is sharper and the deviations from the ellipsoidal shaped droplets are more dramatic. In Figure 3f–j, the initial shape transition from an ellipsoidal droplet to a bulletlike droplet which has a blunt trailing edge can be seen in Figure 3h. At larger capillary numbers, a second transition occurs to a rocket-ship-like shape as seen in Figure 3j. Shown in Figure 3k–n is a highly confined droplet, $C = 1.3$, and droplet radius, $r_d = 66$ μm. This sequence of images illustrates the drop shape transition from an ellipsoid to tails of daughter droplets streaming from the trailing edge of the parent droplet. As the capillary number increases, the droplet progresses from an ellipsoidal shape, as seen in Figure 3k, to a bulletlike shape, Figure 3l, to a droplet with two tails, Figure 3m, and finally to a droplet that breaks up, producing a
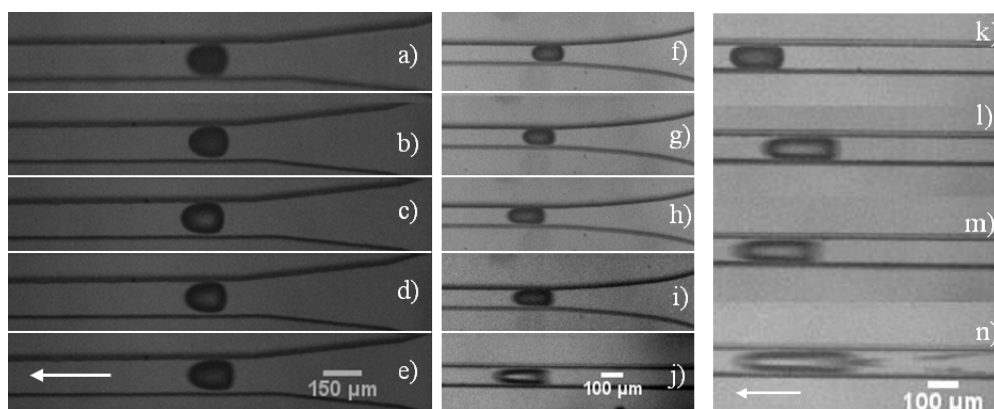
Figure 3. Droplet deformation for a partially confined droplet, $C = 0.9$, and a fully confined droplet, $C = 1.1$, coated with 1 μm amine modified silica particles. Capillary number increases for each series of images from top to bottom. (a−e) Droplet with $C = 0.9$ and $r_d = 66$ μm. (a) $Ca = 0.06$, (b) $Ca = 0.07$, (c) $Ca = 0.09$, (d) $Ca = 0.1$, and (e) $Ca = 0.2$. (f−j) Droplet with $C = 1.1$ and $r_d = 55$ μm. (f) $Ca = 0.02$, (g) $Ca = 0.05$, (h) $Ca = 0.07$, (i) $Ca = 0.1$, and (j) $Ca = 0.2$. (k−n) Droplet deformation for a fully confined droplet, $C = 1.3$ and $r_d = 66$ μm, at various capillary numbers. (k) $Ca = 0.04$, (l) $Ca = 0.09$, (m) $Ca = 0.1$, and (n) $Ca = 0.2$.
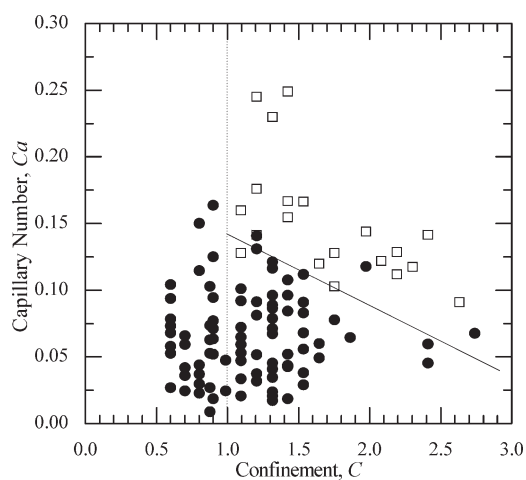

Figure 4. Capillary number as a function of confinement showing when tails (□) form on the rear of the 1 μm particle coated droplets and when they do not form (●). The vertical dotted line shows where droplets become fully confined. The solid line superimposed over the data is not quantitative but meant to emphasize the transition from no tails to tails.

Figure 5. Sequence of images showing tail formation on the trailing edge of a fully confined droplet.

series of daughter droplets, Figure 3n. It appears that the droplets trailing in Figure 3n originate from the breakup of two tails on either side of the droplets trailing edge at the walls. The two tails break off the parent droplet and form daughter droplets, which trail behind the parent droplet and draw additional droplets from the center of the trailing edge of the parent droplet. This illustrates the interplay between the extensional and shear flow in the channel that was seen in ref 9. Interestingly, a very similar transition was seen for droplets covered with surfactants[9] and was likened to the phenomena of tip streaming.[38] However, unlike surfactant covered droplets, in the case of these particle-laden droplets, the formation of tails on the rear of the droplet was only observed for the fully confined cases. It is possible that tails could be observed in the case of the partially confined droplet for much larger capillary numbers. However our experiments were limited to a maximum capillary number of approximately $Ca = 0.25$. It is however likely that particles on the interface of the droplet have formed an elastic shell which resists
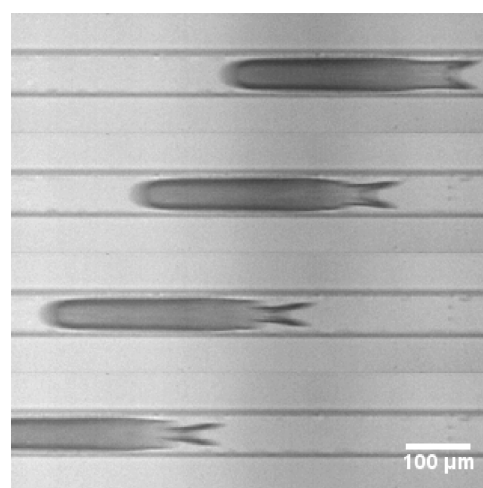
significant droplet deformation and large-scale shape transitions in the absence of confinement. The presence of this elastic shell has additional implications and results in some interesting physical phenomena which will be discussed in greater detail later. Figure 4 is a phase diagram meant to illustrate under what capillary number and confinement conditions tails form on the rear of the 1 μm particle-laden droplets.

A time progression of a large drop entering the hyperbolic contraction is shown in Figure 5 to illustrate the dynamics of tail formation and breakup for particle-laden droplets. Unlike surfactant covered droplets, which were found to produce sharp tails, the droplets in this case form rounded tails that resemble those on a fish. Once formed near the walls, the tails are pulling off from the center of the tailing edge of the droplet, where the extensional forces dominate the flow. The difference in the observed shape of the tails formed on the surfactant covered and particle-laden drops is most likely due in part to the difference in the size of the particles (1 μm) and surfactants (several nanometers) used in previous studies.[9] The relative
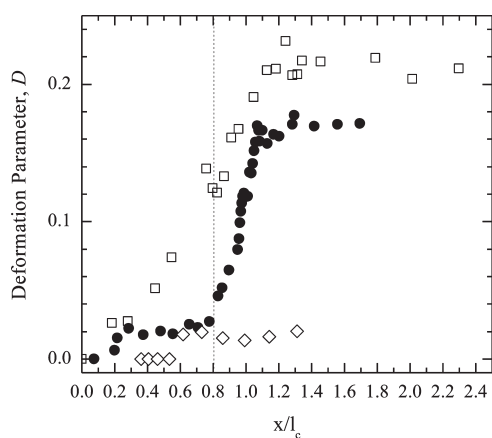
Figure 6. Deformation as a function of position normalized by the length of the hyperbolic contraction for two partially confined droplets, $C = 0.6$ at a capillary number of $Ca = 0.03$ ($\diamond$) and $C = 0.9$ at a capillary number of $Ca = 0.07$ ($\bullet$) and a fully confined droplet $C = 1.1$ at a capillary number of $Ca = 0.06$ ($\square$). The dashed line shows where the transition from partially confined to fully confined for the $C = 1.1$ droplet occurs.
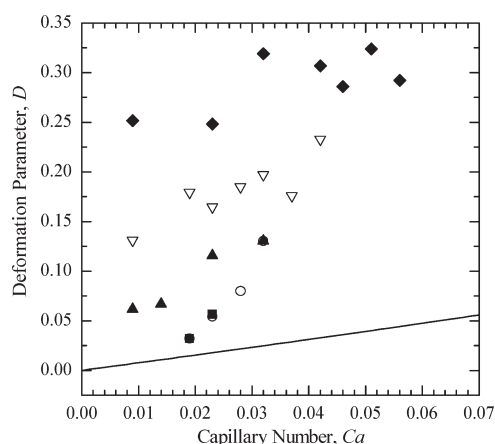

Figure 7. Deformation parameter as a function of the extensional capillary number is shown at various confinements for 500 nm amine modified silica particle coated droplets in oil. The data includes confinements of $C = 0.8$ ($\blacksquare$), $C = 0.9$ ($\bigcirc$), $C = 1.0$ ($\blacktriangle$), $C = 1.1$ ($\square$), and $C = 1.4$ ($\blacklozenge$).

particle size is not negligible when compared to the size of the droplets which are typically on the order of 50 μm in radius. A close analysis of the tails formed in Figures 3k−n and 5 indicates that the radius of curvature of the tail and the ejected daughter drops is of the same order as the silica particles. Additionally, the size and shape of the particles limits the number and packing of particles at the rear stagnation point and thus the effectiveness to which they can locally reduce surface tension and increase droplet curvature. Finally, note that the breakup of particle-laden drops occurs at significantly lower capillary number than that of the confined or unconfined water droplets. However, when compared to surfactant droplets, the breakup occurs at a slightly higher capillary number for a given confinement and the resulting daughter droplets are significantly larger.

To illustrate the effect that confinement has on droplet deformation, the deformation of two partially confined droplets, $C = 0.6$ and $C = 0.9$, at capillary numbers of $Ca = 0.03$ and $Ca = 0.07$, respectively, and a fully confined droplet, $C = 1.1$, at capillary number of $Ca = 0.06$ are shown in Figure 6 as a function of the droplets' position along the contraction. The droplets' position was measured based on the relative position of the leading edge of the droplet with the start of the contraction at $x/l_c = 0$. For these experiments, two different sized hyperbolic contractions were used, FC1 and FC2, and the position of the droplets along the channel was normalized by the contraction length, l_c, for both channels. A value of $x/l_c = 1$ corresponds to the transition from the contraction to the straight extension. For the partially confined droplet with $C = 0.6$, the maximum deformation of $D \cong 0.02$ is reached at $x/l_c = 0.6$. For the partially confined droplet with $C = 0.9$, the droplet reaches maximum deformation at a position of $x/l_c = 1.1$, which is just past the end of the hyperbolic contraction. For the fully confined droplet, the droplet becomes fully confined before reaching the narrowest part of the contraction, at a position of $x/l_c = 0.8$, as shown by the dashed lined in Figure 6. This droplet reaches maximum deformation at $x/l_c = 1.25$, 250 μm after the end of the contraction. For the fully confined case, the droplet deformation increases continuously with position. Thus, in this

case, it is clearly the confinement that dictates the evolution of the drop size and shape and less the strength of the extensional flow. For the partially confined droplets, the deformation does not grow continuously. Instead, the droplet with $C = 0.9$ quickly reaches an asymptotic value of $D \cong 0.02$ before increasing sharply at $x/l_c = 0.8$. This asymptotic value is consistent with the predictions of the Maffetone and Minale model for an unconfined droplet as seen in Figure 2, and the jump in deformation occurs at a point where the droplet confinement is $C = 0.7$ and a transition in shape from ellipsoidal to bulletlike.

To investigate the effect of particle size on droplet deformation and breakup, 500 nm particles were also used to populate the droplet interfaces. Similarly to the 1 μm particle coated droplets, the 500 nm particles showed an increase in droplet deformation as a function of capillary number for any given confinement, as shown in Figure 7. Droplet deformation was found to deviate the predictions of the Maffetone and Minale model for droplets with 500 nm particles adsorbed to the interface. This likely is due to the fact that droplets studied all had a confinement of $C \geq 0.8$ or more. As Figure 6 and our previous studies have shown, confinements above about $C > 0.7$ all show enhanced deformation. When compared to the deformation of droplets coated with 1 μm particles, the deformation induced on droplets with the smaller 500 nm particles is slightly reduced. For example, the 1 μm particle covered droplets with a confinement of $C = 1.4$, droplet deformation ranged from $0.3 \leq D \leq 0.45$ over a range of capillary numbers $0.01 \leq Ca \leq 0.16$. While for the 500 nm particle covered droplets with a confinement of $C = 1.4$ droplet deformation ranged from $0.25 \leq D \leq 0.33$ for the range of capillary numbers from $0.009 \leq Ca \leq 0.06$.

However, even though the degree of deformation was similar for the droplets populated by the 500 nm amine modified silica particles, tails were never observed on the droplets and the droplets were never observed to break up into daughter droplets. Tails were only seen to form for the 1 μm particle laden droplets for a confinement greater than $C > 1$ and a capillary number greater than about $Ca \cong 0.1$. The lack of tail streaming is likely a result of the higher surface tension between the droplets coated with the 500 nm particles and the continuous oil phase and therefore the lower range of capillary numbers accessible within
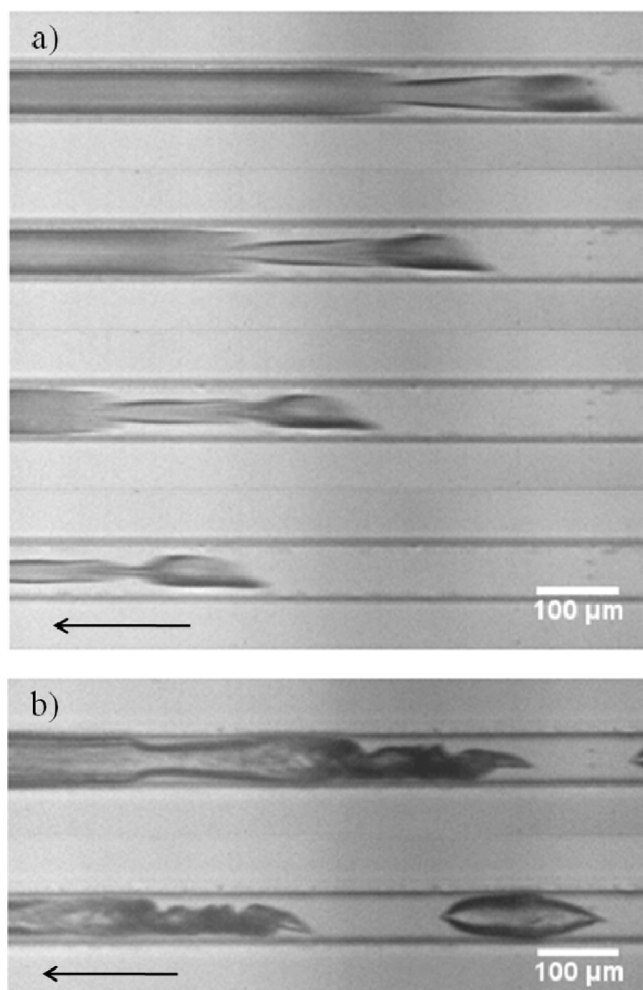
Figure 8. Formation of buckled and crumpled tails. (a) Formation and evolution of a buckled tail. (b) Buckled tail after breakup.

the microfluidic devices. It is likely that tail formation and tail streaming will occur at higher capillary numbers, but unfortunately higher capillary numbers could not be reached within this experimental device design.

For highly confined droplets coated in 1 μm particles, an interesting departure from the tails seen for the fully confined and partially confined droplets occurs. Shown in Figure 8 are droplets for which the elastic particle-laden water—oil interface has buckled. The evolution of the buckling of the interface can be seen prominently in Figure 8a, where a tail is forming and breaking off from the trailing edge of the droplet. At the trailing edge of the droplet, the interface does not return to an ellipsoidal shape as it pinches off. Instead it remains pointed and creased as the particle-laden interface buckles as it begins to retract after pinch-off. In Figure 8b, the process of tail retraction is shown and the evolution of the crumpling interface is illustrated. Note that following the highly confined drop is a daughter drop with a pointed and sharp tail. The sharp points of the daughter droplet and the folded and bent trailing edge of the parent droplet are formed within the contraction and subsequent straight channel. These interface structures are long-lived and can be observed to survive the re-expansion downstream of the hyperbolic contraction.

There is evidence in the literature that, under the right conditions, particle-laden droplets, planar interfaces (frequently called particle rafts, sheets, or monolayers), and cylinders behave like thin elastic films.[39−41] While the dynamics of the interface deformation vary from shape to shape, all these shapes have shown evidence of their elastic nature by undergoing a buckling instability. Buckling instabilities occur when the compressive stress on an elastic membrane exceeds a critical value. In the case of the droplets shown in Figure 8, the compressive load is applied by interfacial tension after daughter drops were produced from a parent drop. In this flow, the elastic membrane is initially stretched by the extensional forces present on the droplet. As the droplet is stretched, new interface is produced and populated by particles. When daughter droplets pinch off or when the deformed drops are allowed to relax downstream of the re-expansion, surface tension drives the drop back toward a spherical droplet and in the process reduces the interfacial area and thereby applies a compressive load on the particle laden interface. Particles, as discussed earlier in this work, are not very mobile and can jam on the interface of the droplets. Unlike surfactants, particles are bound to the interface by thousands of $k_B T$ and are not easily displaced into the water or oil phase. Thus, the droplet must either maintain its nonspherical shape or if the compressive stress exceeds a critical value the droplet will buckle and wrinkle as seen in Figure 8.

■ CONCLUSIONS

In this paper, the deformation and breakup of particle laden droplets in a confined extensional flow was studied using a microfluidic hyperbolic contraction. In these experiments, the effect of confinement is studied to investigate an individual emulsion droplet under conditions that approximate a concentrated emulsion. The deformation of particle coated droplets was found to deviate significantly from the predictions of Maffetone and Minale for unconfined droplets. This deviation is due in part to shear flow superimposed on top of the extensional flow from droplet confinement. Initially, droplets deformed from a spherical- to an ellipsoidal-shaped droplet as predicted by the model. However, at high confinement and capillary numbers, there were a variety of interesting shape transitions observed including bulletlike shapes with a rounded tip and a flattened trailing edge; droplets with one and two tails extending from the back of the droplet from which daughter droplets eventually streamed; and finally, at a very high confinement and capillary number, buckling, wrinkling, and creasing of the droplet interface. This final transition is the result of the finite elasticity of the particle laden membrane which formed along the interface of the droplet as particles jam the surface and has been observed to occur previously on flat particle-laden interfaces.[41] For both surfactant and particle-laden droplets, tail streaming is the result of a local reduction in surface tension at the rear of the droplet due to surfactants or particles being swept by the flow to the rear of the droplet. Although tail streaming has been observed many times in the past for surfactant droplets,[9,32] these observations of tail formation and streaming from the rear of a particle laden droplet are, to our knowledge, the first of their kind.

Droplet deformation was found to increase with increasing confinement and capillary number for both the 1 μm and 500 nm amine modified silica particles studied. The deformation of the droplets was compared to the Maffetone and Minale model for unconfined droplets undergoing pure extensional flow. For the

partially confined droplets, C < 0.7, the deformation was found to follow the Maffetone and Minale model. However, for the nearly fully confined and fully confined droplets, C ≥ 0.9, the droplet deformation deviated strongly from the Maffetone and Minale model within the range of capillary numbers studied. In some cases, droplet deformation was as much as three times that predicted by the Maffetone and Minale model for unconfined droplets. For the nearly fully confined and fully confined droplets, deformation was found to increase with increasing capillary number. For moderately confined droplets, the deformation followed the Maffetone and Minale model until a critical capillary number, after which a strong increase in deformation occurred due to the above-mentioned shape transition. This critical capillary number was found to decrease with increasing confinement.

Droplets which were fully confined and coated in 1 μm silica particles were seen to have tails near the confining walls, for fully confined droplets only. This is in contrast to surfactant droplets for which tail streaming occurred even for partially confined droplets.[9] It is not clear whether full confinement is a necessary requirement for tail formation or if tail formation might happen for lower moderately confined drops if one could reach much larger capillary numbers. These questions are some we hope to answer in the near future. Above a critical capillary number, daughter droplets were produced from these tails. For the 500 nm particle coated droplets, tail streaming was not seen in the range of capillary numbers studied, although it is likely that if higher capillary numbers could have been achieved, droplet breakup would have been observed.

In the case of highly confined droplets, a buckling instability occurred when the daughter droplet pinched off from the parent droplet. As the droplets were deformed from spheres to ellipsoids, the interfacial area grew and was populated by particles. Unlike surfactants, which can easily move from the interface to the bulk, once at the interface particles are kinetically trapped. The compressive stress required for buckling to occur was generated by the pinch off of the daughter droplet, as the interfacial tension acting on the now unconfined daughter droplet acted to drive the droplet toward a spherical shape from its original nonspherical higher surface area shape. The buckled structures were found to be long-lived and were observed to withstand the downstream re-expansion within the microfluidic devices used in this study. It is clear that the elasticity of the jammed particle interface is responsible for the observed buckling, as buckled structures were not seen for surfactant covered droplets.[9]

■ REFERENCES

(1) Shu, L.; Eijkel, J. C. T.; van den Berg, A., Multiphase flow in microfluidic systems - Control and applications of droplets and interfaces. *Adv. Colloid Interface Sci.* **2007**, *133*, 35–49.

(2) McClements, D. J., *Food emulsions: principles, practice and techniques*; CRC Press: Boca Raton, FL, 1999.

(3) Fischer, P.; Erni, P., Emulsion drops in external flow fields - The role of liquid interfaces. *Curr. Opin. Colloid Interface Sci.* **2007**, *12*, 196–205.

(4) Binks, B. P., Particles as surfactants - similarities and differences. *Curr. Opin. Colloid Interface Sci.* **2002**, *7*, 21–41.

(5) Wang, S.; He, Y. J.; Zou, Y., Study of Pickering emulsions stabilized by mixed particles of silica and calcite. *Particuology* **2010**, *8*, 390–393.

(6) Clegg, P. S.; Herzig, E. M.; Schofield, A. B.; Egelhaaf, S. U.; Horozov, T. S.; Binks, B. P.; Cates, M. E.; Poon, W. C. K., Emulsification of partially miscible liquids using colloidal particles: Nonspherical and extended domain structures. *Langmuir* **2007**, *23*, 5984–5994.

(7) Taylor, G. I., The formation of emulsions in definable fields of flow. *Proc. R. Soc. London, Ser. A* **1934**, *146*, 0501–0523.

(8) Mietus, W. G. P.; Matar, O. K.; Lawrence, C. J.; Briscoe, B. J., Droplet deformation in confined shear and extensional flow. *Chem. Eng. Sci.* **2002**, *57*, 1217–1230.

(9) Mulligan, M. K.; Rothstein, J. P., The Effect of Confinement-Induced Shear on Drop Deformation and Breakup in Microfluidic Extensional Flows. *Phys. Fluids* **2011**, *23*, 022004-1–022004-11.

(10) Vananroye, A.; Van Puyvelde, P.; Moldenaers, P., Effect of confinement on the steady-state behavior of single droplets during shear flow. *J. Rheol.* **2007**, *51*, 139–153.

(11) Braisch, B.; Kohler, K.; Schuchmann, H. P.; Wolf, B., Preparation and Flow Behaviour of Oil-In-Water Emulsions Stabilised by Hydrophilic Silica Particles. *Chem. Eng. Technol.* **2009**, *32*, 1107–1112.

(12) Tong, W.; Huang, Y. J.; Liu, C. L.; Chen, X. L.; Yang, Q.; Li, G. X., The morphology of immiscible PDMS/PIB blends filled with silica nanoparticles under shear flow. *Colloid Polym. Sci.* **2010**, *288*, 753–760.

(13) Pickering, S. U., Emulsions. *J. Chem. Soc.* **1907**, *91*, 2001–2021.

(14) Binks, B. P.; Lumsdon, S. O., Stability of oil-in-water emulsions stabilised by silica particles. *Phys. Chem. Chem. Phys.* **1999**, *1*, 3007–3016.

(15) Drelich, A.; Gomez, F.; Clausse, D.; Pezron, I., Evolution of water-in-oil emulsions stabilized with solid particles Influence of added emulsifier. *Colloids Surf., A* **2010**, *365*, 171–177.

(16) Hsu, M. F.; Nikolaides, M. G.; Dinsmore, A. D.; Bausch, A. R.; Gordon, V. D.; Chen, X.; Hutchinson, J. W.; Weitz, D. A., Self-assembled shells composed of colloidal particles: Fabrication and characterization. *Langmuir* **2005**, *21*, 2963–2970.

(17) Reynaert, S.; Moldenaers, P.; Vermant, J., Control over colloidal aggregation in monolayers of latex particles at the oil-water interface. *Langmuir* **2006**, *22*, 4936–4945.

(18) Lin, Y.; Boker, A.; Skaff, H.; Cookson, D.; Dinsmore, A. D.; Emrick, T.; Russell, T. P., Nanoparticle assembly at fluid interfaces: Structure and dynamics. *Langmuir* **2005**, *21*, 191–194.

(19) Fujii, S.; Aichi, A.; Muraoka, M.; Kishimoto, N.; Iwahori, K.; Nakamura, Y.; Yamashita, I., Ferritin as a bionano-particulate emulsifier. *J. Colloid Interface Sci.* **2009**, *338*, 222–228.

(20) Du, K.; Glogowski, E.; Russell, T. E. T. P.; Dinsmore, A. D., Adsorption Energy of Nano- and Microparticles at Liquid-Liquid Interfaces. *Langmuir* **2010**, *26*, 12518–12522.

(21) Pieranski, P., Two-Dimensional Interfacial Colloidal Crystals. *Phys. Rev. Lett.* **1980**, *45*, 569–572.

(22) Lin, Y.; Skaff, H.; Emrick, T.; Dinsmore, A. D.; Russell, T. P., Nanoparticle assembly and transport at liquid-liquid interfaces. *Science* **2003**, *299*, 226–229.

(23) Abate, A. R.; Romanowsky, M. B.; Agresti, J. J.; Weitz, D. A., Valve-based flow focusing for drop formation. *Appl. Phys. Lett.* **2009**, *94*, 023503-1–023503-3.

(24) Abate, A. R.; Weitz, D. A., High-Order Multiple Emulsions Formed in Poly(dimethylsiloxane) Microfluidics. *Small* **2009**, *5*, 2030–2032.

(25) Anna, S. L.; Bontoux, N.; Stone, H. A., Formation of dispersions using "flow focusing" in microchannels. *Appl. Phys. Lett.* **2003**, *82*, 364–366.

(26) Christopher, G. F.; Anna, S. L., Microfluidic methods for generating continuous droplet streams. *J. Phys. D: Appl. Phys.* **2007**, *40*, R319–R336.

(27) Miller, E.; Rotea, M.; Rothstein, J. P., Microfluidic device incorporating closed loop feedback control for uniform and tunable production of micro-droplets and emulsions. *Lab Chip* **2010**, *10*, 1293–1301.

(28) Leal, L. G., *Laminar Flow and Convective Transport Processes: Scaling Principles and Asymptotic Analysis*; Butterworth-Heinemann: Boston, 1992.

(29) Dinsmore, A. D.; Hsu, M. F.; Nikolaides, M. G.; Marquez, M.; Bausch, A. R.; Weitz, D. A., Colloidosomes: Selectively permeable capsules composed of colloidal particles. *Science* **2002**, *298*, 1006–1009.

(30) Sander, J. S.; Studart, A. R., Monodisperse Functional Colloidosomes with Tailored Nanoparticle Shells. *Langmuir* **2011**, *27*, 3301–3307.

(31) Bentley, B. J.; Leal, L. G., An Experimental Investigation of Drop Deformation and Breakup in Steady, Two-Dimensional Linear Flows. *J. Fluid Mech.* **1986**, *167*, 241–283.

(32) De Bruijn, R. A., Tipstreaming of drops in Simple Shear Flows. *Chem. Eng. Sci.* **1993**, *48*, 277–284.

(33) Anderson, J. R.; Chiu, D. T.; Jackman, R. J.; Cherniavskaya, O.; McDonald, J. C.; Wu, H. K.; Whitesides, S. H.; Whitesides, G. M., Fabrication of topologically complex three-dimensional microfluidic systems in PDMS by rapid prototyping. *Anal. Chem.* **2000**, *72*, 3158–3164.

(34) McDonald, J. C.; Duffy, D. C.; Anderson, J. R.; Chiu, D. T.; Wu, H.; Schueller, O. J. A.; Whitesides, G. M., Fabrication of microfluidic systems in poly(dimethylsiloxane). *Electrophoresis* **2000**, *21*, 27–40.

(35) Oliveira, M. S. N.; Alves, M. A.; Pinho, F. T.; McKinley, G. H., Viscous flow through microfabricated hyperbolic contractions. *Exp. Fluids* **2007**, *43*, 437–451.

(36) Randall, G. C.; Schultz, K. M.; Doyle, P. S., Methods to electrophoretically stretch DNA: microcontractions, gels, and hybrid gel-microcontraction devices. *Lab Chip* **2006**, *6*, 516–525.

(37) Maffettone, P. L.; Minale, M., Equation of change for ellipsoidal drops in viscous flow. *J. Non-Newtonian Fluid Mech.* **1998**, *78*, 227–241.

(38) Anna, S. L.; Mayer, H. C., Microscale tipstreaming in a microfluidic flow focusing device. *Phys. Fluids* **2006**, *18*, 121512-1–121512-13.

(39) Datta, S. S.; Shum, H. C.; Weitz, D. A., Controlled Buckling and Crumpling of Nanoparticle-Coated Droplets. *Langmuir* **2010**, *26*, 18612–18616.

(40) Edmond, K. V.; Schofield, A. B.; Marquez, M.; Rothstein, J. P.; Dinsmore, A. D., Stable jets of viscoelastic fluids and self-assembled cylindrical capsules by hydrodynamic focusing. *Langmuir* **2006**, *22*, 9052–9056.

(41) Vella, D.; Aussillous, P.; Mahadevan, L., Elasticity of an interfacial particle raft. *Europhys. Lett.* **2004**, *68*, 212–218.